The WBM Reconfiguration to Prevent the Instability on DC Shipboard Microgrids

Andrea Alessia Tavagnutti
Dept. of Engineering and Architecture
University of Trieste
Trieste, Italy
andreaalessia.tavagnutti@phd.units.it

Daniele Bosich
Dept. of Engineering and Architecture
University of Trieste
Trieste, Italy
dbosich@units.it

Giorgio Sulligoi
Dept. of Engineering and Architecture
University of Trieste
Trieste, Italy
gsulligoi@units.it

***Abstract*—Most innovative DC shipboard microgrids are designed to feed high-performance loads with advanced flexibility feature. The onboard loads not only require great amounts of power, but also their management results dynamically demanding. To this aim, tightly controlled power converters are employed to supply the loads by the filtered DC distribution. In such an islanded system, high-bandwidth converters and LC filters can negatively interact thus finally jeopardizing the ship operation. Smart procedures are to be conceived to preserve the system stability by reconfiguring the online shipboard loads. As the system stability depends on power/bandwidth of each load, the Weighted Bandwidth Method (WBM) is adopted to aggregate the effect of the several controlled loads. Once the WBM identifies two controlled loads as representative of the total dynamics demand, a 3D map results consequent. It reveals the loads combination to be fed without impairing the stability. If the Power Management System (PMS) exploits the outcomes from the 3D map to perform planned reconfigurations, the onboard stable operation is certainly ensured.**

Keywords—DC microgrid, ship, stability, WBM, PMS.

I. Introduction

Environmental concerns and sustainability trend are pushing the marine industry towards a smart electrification [1-2]. In such a context, from the shore connection installations [3-4] to the advanced All Electric Ships (AES) [5], it is evident the need for more efficient and flexible solutions, both for the vessels and the whole marine infrastructure. The adoption of AES can expand the onboard power systems capabilities, and increase the level of integration as well [6-7]. As the upcoming onboard grids include demanding loads and storage solutions, an adequate power distribution is required for their integration. In this regard, the Medium Voltage Direct Current technology [8] appears to be a disruptive key enabler, however characterized by the stability challenge [9-10]. Albeit preventing the instability arise during the system design [11-12], risky conditions can anyway occur during the ship operation. As both loads power and control strategies are dynamically modifiable by the Power Management Systems (PMS) [13], a wrong setting or an excessive demanding condition [14] can force the system operation towards destabilizing scenarios, then triggering instable behaviors and the consequent ship blackout. To ensure the correct system operation, some methodologies can be adopted to foresee the system poles positioning during the ship operation [15-16]. When the instability is predictable, the PMS is consequently trained to just command safe actions on the controlled DC system [17]. This means that only the operations (i.e. changes on power and/or control settings, connection-disconnection of loads, etc.) capable of moving the operating point between stable equilibrium conditions are enabled by the PMS [18]. Differently, the PMS preliminary disables all the actions that are able to transfer the system poles in the right-half plane, thus before their implementation. In a realistic DC shipboard microgrid, not all the loads are high-bandwidth controlled thus ready to destabilize the system operation. The onboard grid also supplies loads with less stringent dynamic constraints. In regarding to the stability issue, the presence of low-bandwidth controlled loads (i.e. stabilizing) have a beneficial effect while compensating for the presence of destabilizing ones [19]. To prevent the arise of instability, the PMS is thus trained for ensuring the proper balance between stabilizing-destabilizing loads. Evidently, this balance is strictly related both on supplied loads and on the requested control bandwidths. Therefore, the PMS is to be employed to coordinate sources and loads, adapting the ship operation to the mission profile [20]. If the PMS is aware of an eventual risk for the ship stability, it can act to avoid the blackout. By reorganizing the supplied loads, it can indeed ensure the balance thus a new stable condition for preventing oscillating behavior and the consequent protections intervention.

The paper explores an advanced functionality to be integrated in the shipboard PMS. Such a new tool is able to assure the DC system stability is case of perturbations on the balance between stabilizing-destabilizing converters. To preserve the system safe-operation, a stability map is built basing on the real-time values from the fed converters (i.e. power/control bandwidth). Such a map defines the DC system stability boundaries, thus the central controller knows how close is the instability for each load configuration. As a consequence, the PMS can reorganize the loads accordingly to the ship mission without harming the system stability. This work presents the stability maps for an exemplifying shipboard DC microgrid. The approach validity is then proven by means of high-fidelity transients from Hardware-In-the-Loop platforms.

II. Shipboard DC Microgrid

The functionality to reconfigure the supplied loads is conceived and tested on the radial DC shipboard grid in Fig. 1.

A. Power System data

The general structure of the controlled microgrid has been already presented in [19], while this paper extends the number of load converters (i.e. right of 6 kV-DC bus). As shown in [19], the generating section on the left is modeled by the Thevenin

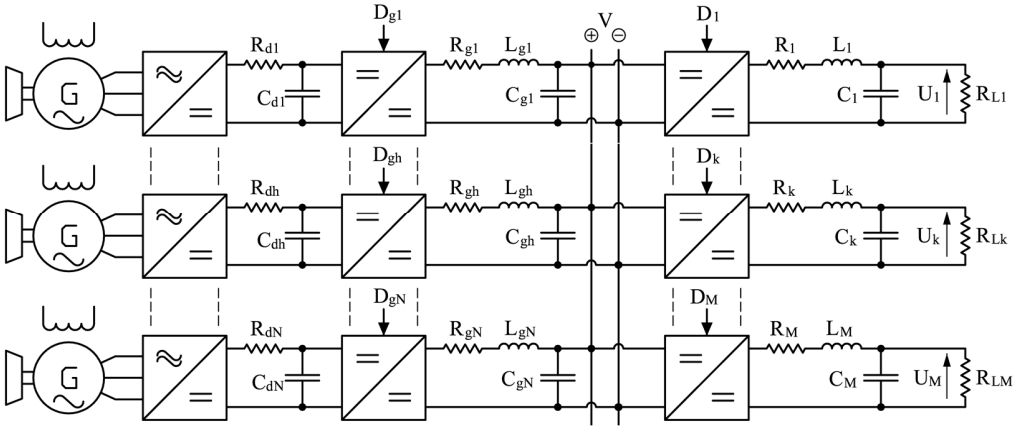

Fig. 1. Multiconverter DC shipboard microgrid [19].

TABLE I. Design data of power system and control, load section.

	k=1	*k=2*	*k=3*	*k=4*	*k=5*	*k=6*	*k=7*	*k=8*
P_{nk} [MW]	3	1	4	1	5	5	3	2
V_n [V]	6000	6000	6000	6000	6000	6000	6000	6000
U_{k0} [V]	4500	3000	5000	5000	4500	3000	5000	5000
D_{k0}	0.75	0.50	0.83	0.83	0.75	0.50	0.83	0.83
I_{k0} [A]	647	320	768	190	647	1600	582	380
f_{sk} [Hz]	3000	3000	3000	3000	3000	3000	3000	3000
$\Delta P_{\%k}$	3	4	4	5	3	4	3	5
$\Delta V_{\%k}$	7	7	7	7	7	7	7	7
$\Delta I_{\%k}$	30	30	30	30	30	30	30	30
R_k [mΩ]	215	391	271	1385	129	78.1	266	693
L_k [mH]	1.9	5.2	1.2	4.9	1.9	1.0	1.6	2.4
C_k [μF]	25.7	19.0	27.4	6.8	25.7	95.2	20.8	13.6
R_{Lk} [Ω]	6.75	9.00	6.25	25.0	4.05	1.8	8.33	12.5
ω_{fk} [rad/s]	4490	3175	5499	5499	4490	3175	5499	5499
ω_k [rad/s]	500	400	200	500	1200	1200	1000	1100

equivalent filter, where L=1.048 mH, C=577.26 μF, ω_0=(LC)$^{-0.5}$. Two conditions are true by assumption. Particularly, the tiny R_{gh} filter resistors are ignored and a notable distance between control bandwidths (h is the subscript for generating converters, k for load converters) and filters resonance frequency is hypothesized, thus ω_h<<ω_k<<ω_{fk}. In these conditions, the equivalent filter can summarize the effect of generating section on the stability matter [19]. The total generating power is 24 MW to be dynamically shared on the eight R_{Lk} onboard loads (i.e. M=8). The latter are supplied from the DC bus (i.e. V_n rated voltage) by means of interfacing DC-DC step-down converters, where P_{nk} is each rated power and D_{k0} is the rated duty cycle (ratio between the output voltage U_{k0} and the input voltage V_n). The design of [21] is adopted to size the eight LC load filters (i.e. R_k, L_k, C_k) whose parameters are in Table I. The authors refer on previous works to explain the parameters meaning.

B. Control Bandwidths on Load Converters

Conventionally, an onboard power grid has low-performing/low-bandwidth controlled loads (e.g. propulsion, services), while others are supposed to operate with high performance/high control bandwidth (e.g. electronics, instrumentation). This feature is also maintained in this paper, where different bandwidths are employed to control the voltage output of interface converters. The ω_k bandwidths are in Table I, where the inequality ω_k<<ω_{fk} is sufficiently verified. The four loads from k=1 to k=4 have bandwidths up to 500 rad/s, while the others even reach the considerable value of 1200 rad/s.

III. Loads Reconfiguration for System Stability

The stability behavior of a DC microgrid is mainly related to the LC input filter and to the power/bandwidth performance on supplied loads. If such an evaluation is quite basic with a single controlled load, the complexity arises when the fed converters are several. In this Section, the Weighted Bandwidth Method (WBM) is used to simplify the stability analysis in a multiple converters DC microgrid, while providing the stability maps as outputs. These maps are adopted to train the PMS in disconnecting the sufficient quota of destabilizing loads. The stability target is consequently preserved.

A. Weighted Bandwidth Method

The WBM is a methodology [19] to verify the DC microgrid stability in feeding the total P_L power on controlled converters. When the loads are many as in ship DC systems, the analytical evaluation of stability is unaffordable. To solve this, the WBM splits the total load conductance G_L=P_L/V_n^2 in two sets based on the bandwidth values. A ω_B bandwidth splitter is defined as in equation (1), where C is the capacitance of generating side equivalent filter and ω_0 its resonance frequency. When an ω_k load converter bandwidth is smaller than the ω_B, the related controlled load populates the S stabilizing set counting M_S loads. Differently, the load is grouped in the D destabilizing set of M_D elements. In total M=M_S+M_D. To evaluate how the M controlled converters affect the DC stability, the WBM concentrates the global impact on the two aggregated loads. From each k-conductance at converter input (i.e. G_k=D_{k0}/R_{Lk}), two total conductances are found in (2). The G_S models the S set controlled by the ω_S bandwidth, which is the weighted equivalent bandwidth of the stabilizing loads, as in (3a). Then, G_D conductance represents the D set with ω_D bandwidth, which is the weighted equivalent bandwidth of the destabilizing loads, as in (3b). The m_k term is the ratio among the single G_k and the set conductance, e.g. m_1=G_1/G_S. By studying the interaction between the input filter and the two aggregated loads, the stability is assessed as in III.B.

$$\omega_B = \frac{-G_L + \sqrt{G_L^2 + 4C^2\omega_0^2}}{2C} \tag{1}$$

$$\begin{cases} P_L = \sum_{k=1}^{M} P_k = \sum_{k=1}^{MS} P_k + \sum_{k=MS+1}^{M} P_k = P_S + P_D \\ G_L = \sum_{k=1}^{M} G_k = \sum_{k=1}^{MS} G_k + \sum_{k=MS+1}^{M} G_k = G_S + G_D \end{cases} \tag{2}$$

$$\begin{cases} \omega_S = \sum_{k=1}^{MS} m_k \omega_k & (3a) \\ \omega_D = \sum_{k=MS+1}^{M} m_k \omega_k & (3b) \end{cases}$$

$$\begin{cases} \Im\left(\overline{Z_o} \cdot \overline{Y_i}\right) = -\frac{\omega_{cr}}{C\left(\omega_0^2 - \omega_{cr}^2\right)} \cdot \left[G_S \frac{\omega_S^2 - \omega_{cr}^2}{\omega_S^2 + \omega_{cr}^2} + G_D \frac{\omega_D^2 - \omega_{cr}^2}{\omega_D^2 + \omega_{cr}^2} \right] = 0 & (4a) \\ \Re\left(\overline{Z_o} \cdot \overline{Y_i}\right) = -\frac{2\omega_{cr}^2}{C\left(\omega_0^2 - \omega_{cr}^2\right)} \cdot \left[G_S \frac{\omega_S}{\omega_S^2 + \omega_{cr}^2} + G_D \frac{\omega_D}{\omega_D^2 + \omega_{cr}^2} \right] = -\Psi & (4b) \end{cases}$$

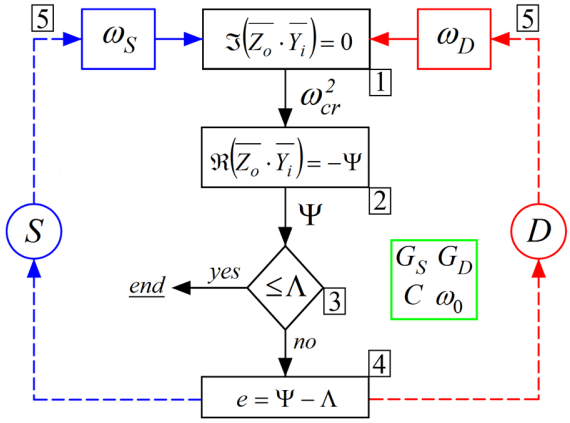

Fig. 2. Stability assessment iterative process [19].

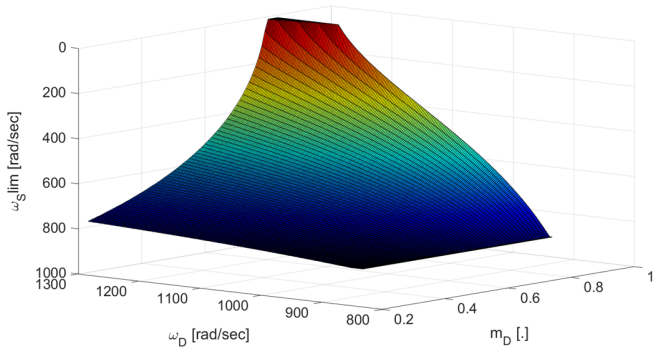

Fig. 3. 3D stability map, P_L=24 MW and ω_B=832 rad/s.

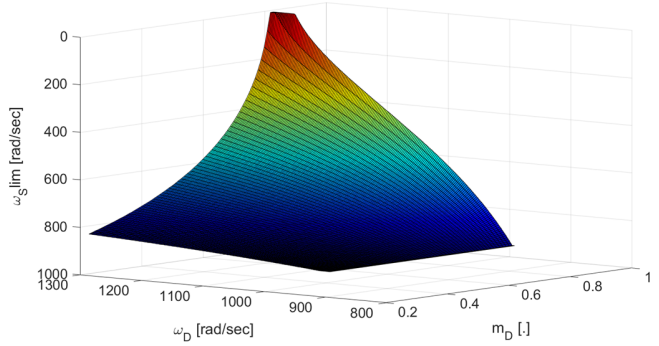

Fig. 4. 3D stability map, P_L=20 MW and ω_B=892 rad/s.

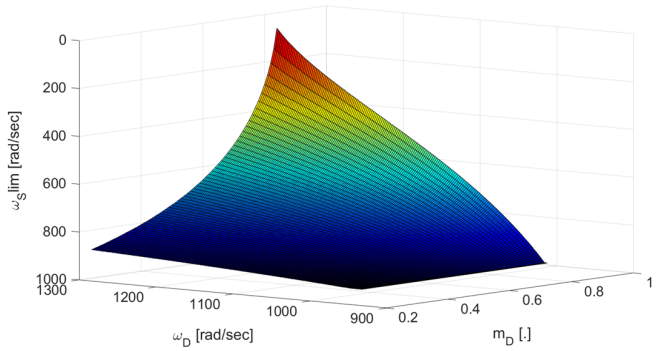

Fig. 5. 3D stability map, P_L=17.5 MW and ω_B=932 rad/s.

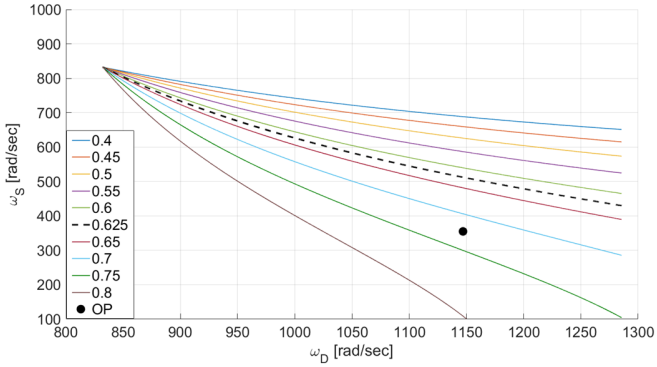

Fig. 6. 2D stability map, P_L=24 MW and ω_B=832 rad/s.

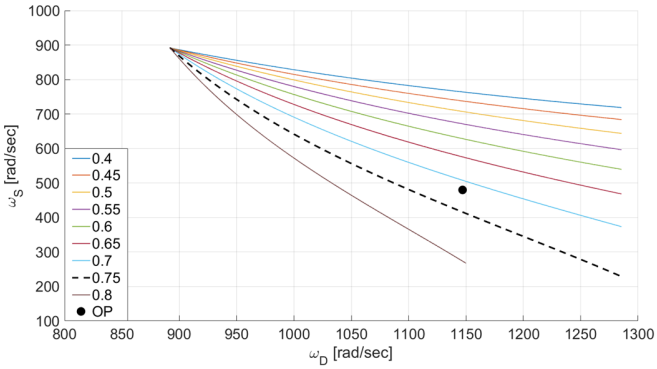

Fig. 7. 2D stability map, P_L=20 MW and ω_B=892 rad/s.

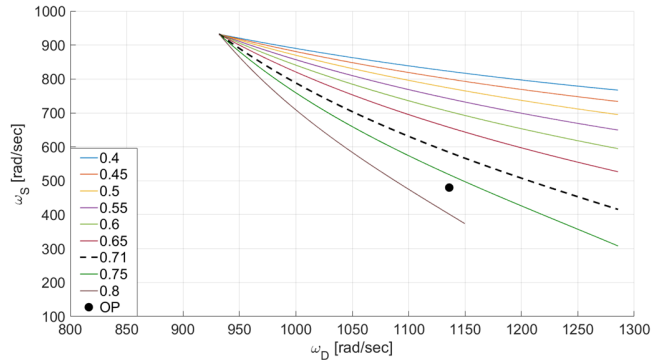

Fig. 8. 2D stability map, P_L=17.5 MW and ω_B=932 rad/s.

B. Stability Assessment

By applying the WBM, the loads effect is concentrated in only two sets, then the DC stability is assessable on the output impedance-input admittance as in [19]. Same approach also in the process of Fig. 2, where the stability is tested for a set of microgrid data (i.e. green box). The Nyquist criterion (4a)-(4b) is applied to verify that the curve $Z_0(j\omega)\cdot Y_i(j\omega)$ does not clockwise-encircle the point (−1,0) on the Gauss plane. In this case, the term Ψ in (4b) results less than 1. By replaying the same process for a range of variation in m_D-ω_D, the 3D stability maps are consequent in Figs. 3-5. Two inputs identify the X-Y axes. On X axis the ratio m_D, which models the destabilizing conductance as $G_D=m_D\cdot G_L$. On Y axis, the ω_D input moves from ω_B to ω_0, above which the stability is certainly lost [22]. By discretizing the axes-ranges, the assessment is iterated to find the $\omega_{S\text{lim}}$. For each couple m_D-ω_D, the latter is the maximum stabilizing bandwidth beyond which the WBM-based model is instable, thus ψ=1 when $\omega_S=\omega_{S\text{ lim}}$. By cutting the 3D solids with m_D vertical planes, the 2D maps in Figs. 6-8 are the result.

C. PMS activity for stability warranty

The 2D maps are the starting point on which set up the PMS learning. When the PMS has the knowledge on the stability balance, its activity is properly trained to make feasible only safe actions on the DC microgrid. Such actions (e.g. load connection/disconnection) are the ones that force the shipboard operation towards stable operating points. Conversely, all the operations that lead to instability are banned before their implementation. The first example in Fig. 6 is the condition in which the PMS starts its operation, where the fed loads are in Table I. Both powers and bandwidths are already defined, as well as the ω_B term (832 rad/s) to split the controlled loads in the two *S*-*D* sets. The total P_L is 24 MW, while the destabilizing bandwidth is ω_D=1147 rad/s. As in (3b), last value considers the m_k load power partition and the bandwidths of most performing converters, thus 5-6-7-8. Conversely, the remaining converters (i.e. 1-2-3-4) populate the *S* set, whose representative load is controlled by the ω_S=355 rad/s (3a). Being 15 MW the total power on destabilizing loads, the m_D=15/24=0.625 identifies the dashed limit line in the 2D stability map. As the ω_D-ω_S point of intersection is below the stability border, the stability is ensured as the ψ real part is certainly lower than 1. From this initial condition, the stabilizing load 3 is disconnected (Fig. 7) to satisfy the ship operative request, while other loads are not modified neither in bandwidths nor in power. This action does not largely move the ω_B, equal to 892 rad/s. Such a value still recognizes 5-6-7-8 as destabilizing loads, whilst 1-2-4 are now the only able to stabilize the DC system. The ω_D is again equal to 1147 rad/s, while the m_D goes up to 15/20=0.75 to evaluate the power-off on stabilizing converter 3. When cutting 4 MW from the lowest bandwidth converter, the total P_L is 20 MW while the increased ω_S reaches the value of 480 rad/s. As the ω_D-ω_S intersection is above the dashed line, the reduced stabilizing quota is insufficient to balance the destabilizing loads. As ψ>1, the instability/blackout is inescapable. To avoid this, the disconnection on stabilizing loads must be preempted by a power-off on destabilizing loads. The Fig. 8 depicts a case

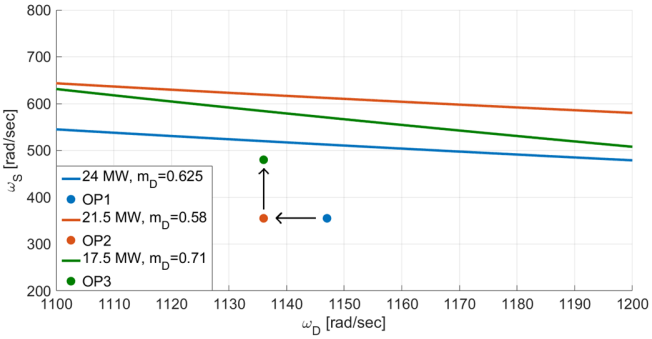

Fig. 9. Operating points transition on 2D stability map.

where the PMS preventive action on *D* can ensure the *S*-*D* balance even after the power-off on *S*. By beforehand removing 2.5 MW on the destabilizing load 5, the following 4 MW reduction on *S* is doable as the final ω_D-ω_S point is below the dashed limit of m_D=12.5/17.5=0.71. In Fig. 9, the stability maps indeed enables the PMS feasible load reconfigurations from OP1 to OP3. The PMS is trained to drive towards the OP3 by forcing the transition through the OP2 stable operating point.

IV. Validation by Real-time Emulation

The Section IV is aimed at verifying how the WBM reconfiguration can prevent the system instability. By following the operating points transition in Section III, some emulations on Typhoon HIL platform will be performed to testify underdamped transients after the problematic disconnection of a stabilizing load. Such a perturbation is firstly classified as critical as it potentially moves the DC microgrid towards the system instability. Then, a training on the PMS will demonstrate its efficacy in redefining the balance of stabilizing-destabilizing loads. Even after the power-off of a crucial low-bandwidths controlled converter, the reconfigured DC grid will indeed behave in a stable way, while avoiding the blackout.

A. Hardware In the Loop platform

To evaluate the system stability after the stabilizing load disconnection, a testbed is configured on Typhoon HIL platform. Its schematic implementation is given in Fig. 10. The generating converters are modeled as ideal voltage sources and their output filters are grouped together (left side of Fig.10) with the Thevenin equivalent (i.e. *L*=1.048 mH, *C*=577.26 μF). In the right part of Fig. 10, the eight controlled DC-DC load converters are supplied by the DC bus having 6000 V as rated value. Their control bandwidths as well as the load powers are in Table I. The eight power converters are emulated on the Typhoon HIL 604 platform by adopting three cores among the eight available, then implementing the core coupling elements in Fig. 10. The real-time emulations run with a time-step of 0.5 us, while the results in the figures are depicted each 1 ms. As the emulation goal is not on power converters functionality, instead on stability balance, simple buck converters (i.e. only one switch) are considered effective in this test. Although the load filters are neglected in the stability analysis to reduce the study complexity, they are conversely modeled as in Table I for the HIL test (output filters of load converters in Fig. 10). Also

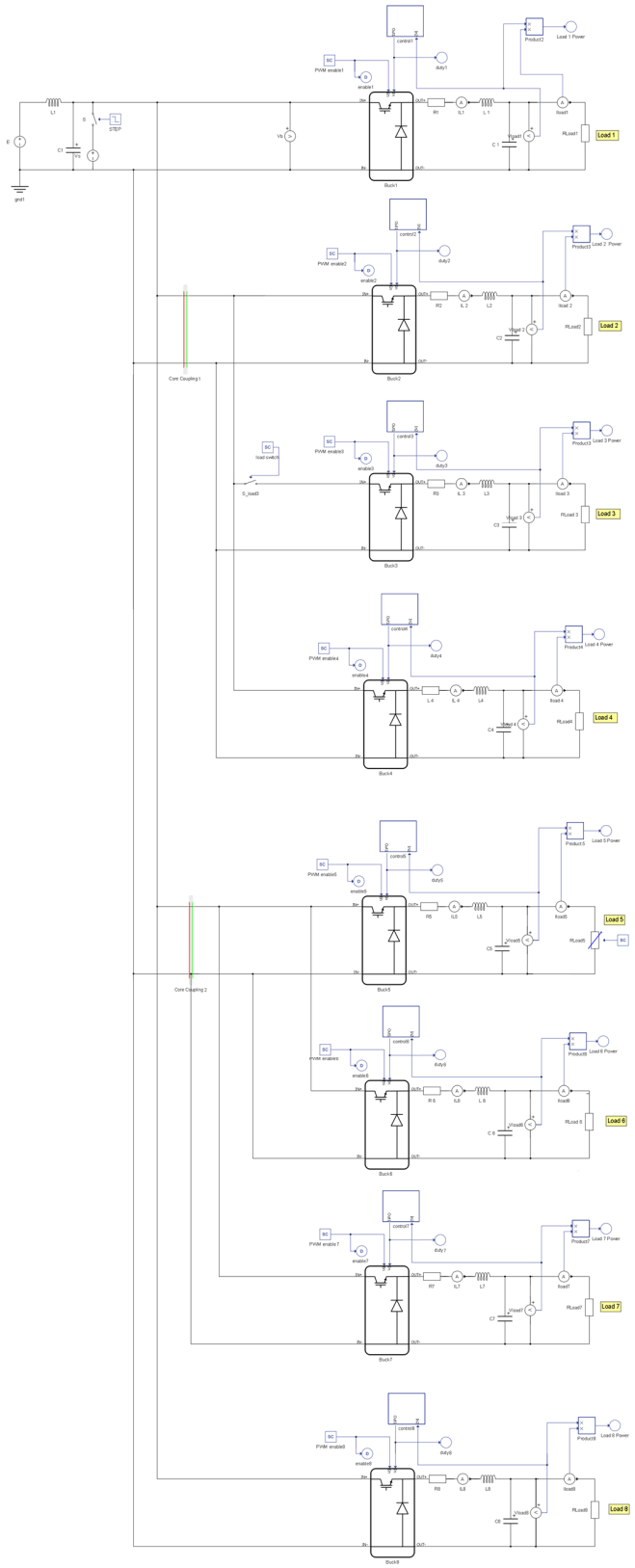

Fig. 10. Testbed on Typhoon HIL 604.

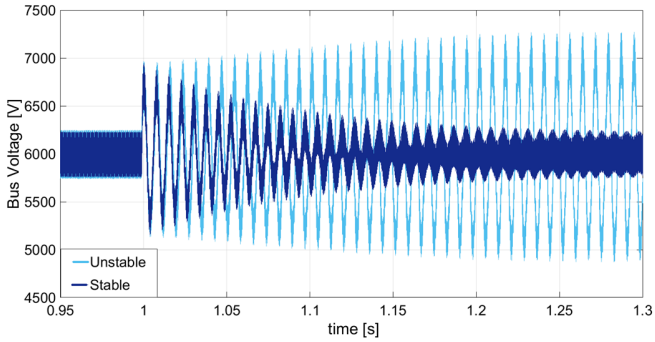

Fig. 11. Bus voltage transients, stable and unstable case.

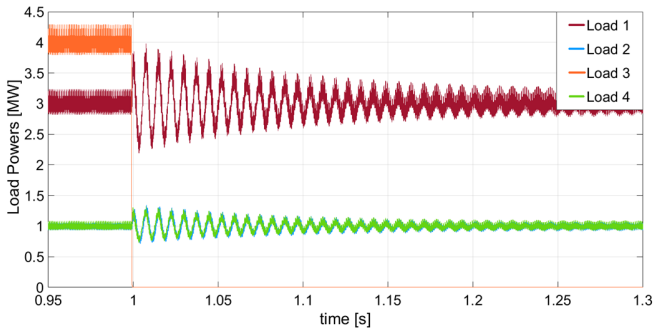

Fig. 12. Load power transients, stabilizing loads.

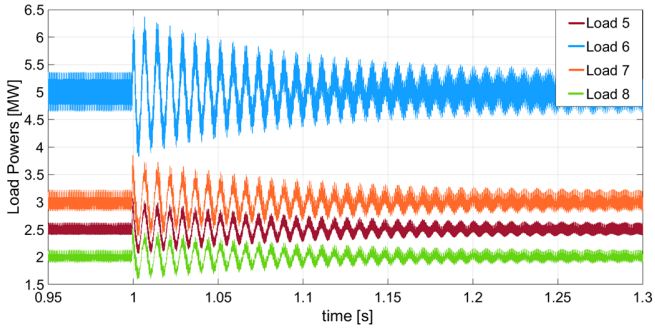

Fig. 13. Load power transients, destabilizing loads.

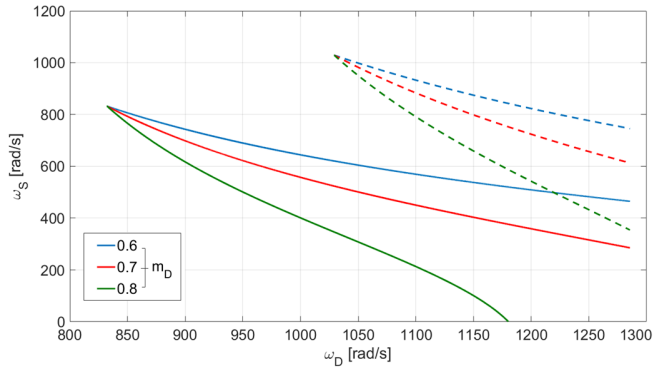

Fig. 14. Effect of total power variation in stability map translation (solid line P_L=24 MW, dashed line P_L=12 MW).

the integral controllers adopted in the stability assessment [19] are slightly modified as PI controllers to increase the fidelity of HIL emulation. The testbed constitutes a Software HIL, an emulating environment to prove the WBM theory.

B. Test on stabilizing load disconnection

Some HIL tests verify the effects of WBM reconfiguration. The transients in Figs. 11-13 prove how a smart transition over the operating points avoids the stability unbalance, then enabling the programmed disconnection of load 3. At the beginning of the test, the system works at steady-state and its stability map is in Fig. 6. If at 1 s the PMS simply disconnects the 4 MW of load 3, the power system become unstable, as in the cyan transient of Fig. 11. Indeed, the operating point is above the stability boundary in the stability map of that final condition (Fig. 7). Conversely, a trained PMS checks the 2D maps to decide the preemptive power-decrease (from 5 MW to 2.5 MW) on destabilizing load 5, before disconnecting load 3. As in the blue transient of Fig. 11, this reduction is sufficient to assure stability, highlighted also in the power transients of Figs. 12-13. This final stability condition is in Fig. 8, where the operating point is below the stability boundary. The switching results demonstrate how this reconfiguration approach can extend the stable operating conditions of DC microgrids. As the PMS is trained to disconnect the smallest destabilizing quota, most of demanding loads can still be fed also without a large stabilizing contribution. Finally, the Fig. 14 shows how the 2D stability margins change when decreasing the total load power. When the load demand is lower (dashed lines with half power), the ω_D bandwidth can increase while maintaining the stability target.

V. Conclusions

In the tomorrow DC microgrids on ships, the undesired resonance among high-bandwidth converters and LC filters triggers unstable phenomena, then the consequent system blackout. Conversely, the supply of low-bandwidth converters balances the effect of destabilizing loads, then ensuring the uninterrupted system operation. In this paper, the Weighted Bandwidth Method (WBM) evaluates how the exploitation of this compensating action can improve the stability of an isolated radial DC grid. The WBM adoption reduces the complexity of DC stability analysis, while revealing the 2D maps. The latter identify the load converters configurations (i.e. power/bandwidth) for which the DC system stability is preserved. The so-obtained stability maps are then integrated in the control system of the DC system. These maps are highly important, as they are capable of suggesting the safe-stable configuration of loads. From the knowledge of these maps, the PMS can be trained to perform planned reconfigurations to constantly guarantee the stability requirement. In this work, the disconnection of a large stabilizing load is the case on which the WBM reconfiguration is tested by means of HIL emulations. The compliance between the outcomes from 2D maps and the real-time transients confirms the value of the proposed approach.

Acknowledgment

The authors would like to thank Typhoon HIL for providing the platform used in the development of this research work.

References

[1] L. Xu et al., "A Review of DC Shipboard Microgrids Part I: Power Architectures, Energy Storage and Power Converters," in *IEEE Transactions on Power Electronics*.

[2] A. J. Sorensen et al., "Toward Safer, Smarter, and Greener Ships: Using Hybrid Marine Power Plants," in *IEEE Electrification Magazine*, vol. 5, no. 3, pp. 68-73, Sept. 2017.

[3] G. Sulligoi, D. Bosich, R. Pelaschiar, G. Lipardi and F. Tosato, "Shore-to-Ship Power," in *Proceedings of the IEEE*, vol. 103, no. 12, pp. 2381-2400, Dec. 2015.

[4] A. Rolán, P. Manteca, R. Oktar and P. Siano, "Integration of Cold Ironing and Renewable Sources in the Barcelona Smart Port," in *IEEE Trans. on Industry Applications*, vol. 55, no. 6, pp. 7198-7206, Nov.-Dec. 2019.

[5] S. Fang, Y. Wang, B. Gou and Y. Xu, "Toward Future Green Maritime Transportation: An Overview of Seaport Microgrids and All-Electric Ships," in *IEEE Transactions on Vehicular Technology*, vol. 69, no. 1, pp. 207-219, Jan. 2020.

[6] T. Ericsen, "The ship power electronic revolution: Issues and answers," *Proc. 2008 55th IEEE Petroleum and Chemical Industry Technical Conference*, 2008, pp. 1-11.

[7] E. Skjong, R. Volden, E. Rødskar, M. Molinas, T. A. Johansen and J. Cunningham, "Past, Present, and Future Challenges of the Marine Vessel's Electrical Power System," in *IEEE Transactions on Transportation Electrification*, vol. 2, no. 4, pp. 522-537, Dec. 2016.

[8] N. Zohrabi, J. Shi, S. Abdelwahed, "An overview of design specifications and requirements for the MVDC shipboard power system", *Int. Journal of Elec. Power & Energy Systems*, Volume 104, 2019.

[9] A. A. Tavagnutti, D. Bosich and G. Sulligoi, "A Multi-Model Methodology for Stability Assessment of Complex DC Microgrids," *Proc. 2021 IEEE ICDCM*, 2021, pp. 1-7.

[10] X. Zhu, H. Hu, H. Tao, Z. He and R. M. Kennel, "Stability Prediction and Damping Enhancement for MVdc Railway Electrification System," in *IEEE Trans. on Ind. Appl.*, vol. 55, no. 6, pp. 7683-7698, Nov.-Dec. 2019.

[11] "IEEE Recommended Practice for 1 kV to 35 kV Medium-Voltage DC Power Systems on Ships," in *IEEE Std 1709-2018 (Revision of IEEE Std 1709-2010)* , vol., no., pp.1-54, 7 Dec. 2018.

[12] P. Liutanakul, A. Awan, S. Pierfederici, B. Nahid-Mobarakeh and F. Meibody-Tabar, "Linear Stabilization of a DC Bus Supplying a Constant Power Load: A General Design Approach," in *IEEE Transactions on Power Electronics*, vol. 25, no. 2, pp. 475-488, Feb. 2010.

[13] S. Kotra and M. K. Mishra, "A Supervisory Power Management System for a Hybrid Microgrid With HESS," in *IEEE Transactions on Industrial Electronics*, vol. 64, no. 5, pp. 3640-3649, May 2017.

[14] S. Faddel, A. A. Saad, M. E. Hariri and O. A. Mohammed, "Coordination of Hybrid Energy Storage for Ship Power Systems With Pulsed Loads," in *IEEE Transactions on Industry Applications*, vol. 56, no. 2, pp. 1136-1145, March-April 2020.

[15] I. Cvetkovic, Z. Liu, D. Boroyevich and R. Burgos, "On-line Measurement of Inward and Outward Impedances for Stability Assessment," *Proc. 2019 IEEE ESTS*, 2019, pp. 113-118.

[16] A. Riccobono and E. Santi, "Stability analysis of an all-electric ship MVDC Power Distribution System using a novel Passivity-Based Stability Criterion," *Proc. 2013 IEEE ESTS*, 2013, pp. 411-419.

[17] P. Xie et al., "Optimization-Based Power and Energy Management System in Shipboard Microgrid: A Review," in *IEEE Systems Journal*, vol. 16, no. 1, pp. 578-590, March 2022.

[18] W. Du, G. Yang, C. Pan and P. Xi, "A Heterogeneous Multi-Agent System Model With Navigational Feedback for Load Demand Management of a Zonal Medium Voltage DC Shipboard Power System," in *IEEE Access*, vol. 7, pp. 148073-148083, 2019.

[19] D. Bosich, G. Giadrossi, S. Pastore, and G. Sulligoi, "Weighted Bandwidth Method for Stability Assessment of Complex DC Power Systems on Ships," *Energies*, vol. 15, no. 1, p. 258, Dec. 2021.

[20] F. Kanellos, A. Anvari-Moghaddam, and J. Guerrero, "Smart Shipboard Power System Operation and Management," *Inventions*, vol. 1, no. 4, p. 22, Nov. 2016.

[21] D. Bosich, M. Gibescu and G. Sulligoi, "Large-signal stability analysis of two power converters solutions for DC shipboard microgrid," *Proc. 2017 IEEE ICDCM*, 2017, pp. 125-132.

[22] S. Pastore, D. Bosich and G. Sulligoi, "A frequency analysis of the small-signal voltage model of a MVDC power system with two cascade DC-DC converters," *2018 IEEE ESARS-ITEC*, 2018, pp. 1-6.